

# Modeling gravitational recoil from precessing highly-spinning unequal-mass black-hole binaries

Carlos O. Lousto and Yosef Zlochower

*Center for Computational Relativity and Gravitation,  
School of Mathematical Sciences, Rochester Institute of Technology,  
78 Lomb Memorial Drive, Rochester, New York 14623*

(Dated: November 29, 2018)

We measure the gravitational recoil for unequal-mass-black-hole-binary mergers, with the larger BH having spin  $a/m^H = 0.8$ , and the smaller BH non-spinning. We choose our configurations such that, initially, the spins lie on the orbital plane. The spin and orbital plane precess significantly, and we find that the out-of plane recoil (i.e. the recoil perpendicular to the orbital plane around merger) varies as  $\eta^2/(1+q)$ , in agreement with our previous prediction, based on the post-Newtonian scaling.

PACS numbers: 04.25.Dm, 04.25.Nx, 04.30.Db, 04.70.Bw

## I. INTRODUCTION

The recent observational discovery of a possible recoiling supermassive black hole at a speed of  $2650 \text{ km s}^{-1}$  with respect to its host galaxy [1] represent the first observational evidence in support of the predictions of General Relativity in the strong-field, highly-dynamical, and highly-nonlinear regime. This recoil, if it in fact resulted from a black-hole merger, would confirm the theoretical prediction of Campanelli et al. [2] that black-hole mergers can lead to very large recoils. This original prediction, and the subsequent calculation [3] that indicated that such recoils can be as large as  $4000 \text{ km s}^{-1}$ , has been a key trigger for these astronomical searches.

Thanks to recent breakthroughs in the full non-linear numerical evolution of black-hole-binary spacetimes [4, 5, 6], it is now possible to accurately simulate the merger process and examine its effects in this highly non-linear regime [7, 8, 9, 10, 11, 12, 13, 14, 15, 16, 17, 18, 19, 20, 21]. Black-hole binaries will radiate between 2% and 8% of their total mass and up to 40% of their angular momenta, depending on the magnitude and direction of the spin components, during the merger [9, 10, 11]. In addition, the radiation of net linear momentum by a black-hole binary leads to the recoil of the final remnant hole [2, 3, 22, 23, 24, 25, 26, 27, 28, 29, 30, 31, 32, 33, 34, 35, 36, 37, 38, 39, 40, 41, 42, 43], which can have astrophysically important effects [2, 41, 44, 45, 46, 47].

In [2] we introduced the following heuristic model for the gravitational recoil of a merging binary.

$$\vec{V}_{\text{recoil}}(q, \vec{\alpha}_i) = v_m \hat{e}_1 + v_{\perp} (\cos(\xi) \hat{e}_1 + \sin(\xi) \hat{e}_2) + v_{\parallel} \hat{e}_z, \quad (1)$$

where

$$v_m = A \frac{\eta^2(1-q)}{(1+q)} (1+B\eta), \quad (2a)$$

$$v_{\perp} = H \frac{\eta^2}{(1+q)} (\alpha_2^{\parallel} - q\alpha_1^{\parallel}), \quad (2b)$$

$$v_{\parallel} = K \cos(\Theta - \Theta_0) \frac{\eta^2}{(1+q)} |\vec{\alpha}_2^{\perp} - q\vec{\alpha}_1^{\perp}|, \quad (2c)$$

$A = 1.2 \times 10^4 \text{ km s}^{-1}$  [27],  $B = -0.93$  [27],  $H = (6.9 \pm 0.5) \times 10^3 \text{ km s}^{-1}$ ,  $\vec{\alpha}_i = \vec{S}_i/m_i^2$ ,  $\vec{S}_i$  and  $m_i$  are the spin and mass of hole  $i$ ,  $q = m_1/m_2$  is the mass ratio of the smaller to larger mass hole,  $\eta = q/(1+q)^2$  is the symmetric mass ratio, the index  $\perp$  and  $\parallel$  refer to perpendicular and parallel to the orbital angular momentum respectively at the effective moment of the maximum generation of the recoil (around merger time),  $\hat{e}_1, \hat{e}_2$  are orthogonal unit vectors in the orbital plane, and  $\xi$  measures the angle between the “unequal mass” and “spin” contributions to the recoil velocity in the orbital plane. The angle  $\Theta$  was defined as the angle between the in-plane component of  $\vec{\Delta} \equiv (m_1+m_2)(\vec{S}_2/m_2 - \vec{S}_1/m_1)$  and the infall direction at merger. The form of Eq. (2a) was proposed in [27, 48], while the form of Eqs. (2b) and (2c) was proposed in [2] based on the post-Newtonian expressions in [49]. In Ref [3] we determined that  $K = (6.0 \pm 0.1) \times 10^4 \text{ km s}^{-1}$ , and made the first prediction that the maximum possible recoil is  $\sim 4000 \text{ km s}^{-1}$  for equal-mass binaries with anti-parallel spins in the orbital plane (in Ref. [43], we performed simulations with a measured recoil of  $3250 \text{ km s}^{-1}$ ). Although  $\xi$  may in general depend strongly on the configuration, the results of [33] and post-Newtonian calculations show that  $\xi$  is  $90^\circ$  for head-on collisions, and the results presented in Ref. [50] indicate that  $\xi \sim 145^\circ$  for a wide range of quasi-circular configurations. A simplified version of Eq. (1) that models the magnitude of  $V_{\text{recoil}}$  was independently proposed in [34], and a simplified form of Eq. (2b) for the equal-mass aligned spin case was proposed in [32]. A more general formula, using only symmetry arguments and fits to numerical data, was recently proposed in [51, 52].

Our heuristic formula (1) describing the recoil velocity of a black-hole binary remnant as a function of the parameters of the individual holes has been theoretically verified in several ways. In [3] the  $\cos \Theta$  dependence was established and was confirmed in [38] for binaries with different initial separations. In Ref. [37] the decomposi-

tion into spin components perpendicular and parallel to the orbital plane was verified, and in [42] it was found that the quadratic-in-spin corrections to the in-plane recoil velocity are less than  $20 \text{ km s}^{-1}$ . Recently, Baker et al. [53] measured the recoil for unequal-mass, spinning binaries, with spins lying in the initial orbital plane, and concluded that the leading order dependence of the out-of-plane kick was  $\mathcal{O}(\eta^3)$ , rather than the  $\mathcal{O}(\eta^2)$  that we predicted. In this paper we examine this dependence in detail.

As pointed out in [53] the consequences of an  $\mathcal{O}(\eta^3)$  dependence of the recoil, rather than an  $\mathcal{O}(\eta^2)$  dependence, are significant for both the retention of intermediate mass black holes (IMBH) in globular clusters and supermassive black holes in galaxies. It is thus important that we understand how the recoil depends on mass ratio.

In their paper, Baker et al. [53] analyzed configurations that required fitting two angle parameters (for a given value of  $q$ ) before the maximum recoil could be obtained. Their configuration also produced very small recoil velocities for smaller values of  $q$ . In order to help simplify the dependence, we choose configurations that only require fitting one angle parameter in Eq. (2c), and have a substantial recoil even for our smallest mass ratios.

The paper is organized as follows, in Sec. II we review the numerical techniques used for the evolution of the black-hole binaries and the analysis of the physical quantities extracted at their horizons, in Sec. III we present results and analysis, and in Sec. IV we present our conclusions.

## II. TECHNIQUES

To compute initial data, we use the puncture approach [54] along with the TWOPUNCTURES [55] thorn. In this approach the 3-metric on the initial slice has the form  $\gamma_{ab} = (\psi_{BL} + u)^4 \delta_{ab}$ , where  $\psi_{BL}$  is the Brill-Lindquist conformal factor,  $\delta_{ab}$  is the Euclidean metric, and  $u$  is (at least)  $C^2$  on the punctures. The Brill-Lindquist conformal factor is given by  $\psi_{BL} = 1 + \sum_{i=1}^n m_i^p / (2|\vec{r} - \vec{r}_i|)$ , where  $n$  is the total number of ‘punctures’,  $m_i^p$  is the mass parameter of puncture  $i$  ( $m_i^p$  is *not* the horizon mass associated with puncture  $i$ ), and  $\vec{r}_i$  is the coordinate location of puncture  $i$ . We evolve these black-hole-binary data-sets using the LAZEV [56] implementation of the moving puncture approach [5, 6]. In our version of the moving puncture approach we replace the BSSN [57, 58, 59] conformal exponent  $\phi$ , which has logarithmic singularities at the punctures, with the initially  $C^4$  field  $\chi = \exp(-4\phi)$ . This new variable, along with the other BSSN variables, will remain finite provided that one uses a suitable choice for the gauge. An alternative approach uses standard finite differencing of  $\phi$  [6]. Recently Marronetti et al. [60] proposed the use of  $W = \sqrt{\chi}$  as an evolution variable. For the runs presented here we use centered, eighth-order finite differencing in space [61] and an RK4 time integrator (note that we do

not upwind the advection terms).

We use the Carpet [62] mesh refinement driver to provide a ‘moving boxes’ style mesh refinement. In this approach refined grids of fixed size are arranged about the coordinate centers of both holes. The Carpet code then moves these fine grids about the computational domain by following the trajectories of the two black holes.

We obtain accurate, convergent waveforms and horizon parameters by evolving this system in conjunction with a modified 1+log lapse and a modified Gamma-driver shift condition [5, 63], and an initial lapse  $\alpha(t = 0) = 2/(1 + \psi_{BL}^4)$ . The lapse and shift are evolved with

$$(\partial_t - \beta^i \partial_i) \alpha = -2\alpha K \quad (3a)$$

$$\partial_t \beta^a = B^a \quad (3b)$$

$$\partial_t B^a = 3/4 \partial_t \tilde{\Gamma}^a - \sigma B^a. \quad (3c)$$

Note that we denote the Gamma-driver parameter by  $\sigma$  rather than the more typical  $\eta$  to avoid confusion with the symmetric mass ratio parameter. These gauge conditions require careful treatment of  $\chi$ , the inverse of the three-metric conformal factor, near the puncture in order for the system to remain stable [5, 7, 15]. In our tests,  $W$  showed better behavior at very early times ( $t < 10M$ ) (i.e. did not require any special treatment near the punctures), but led to evolutions with lower effective resolution when compared to  $\chi$ . Interestingly, a mixed evolution system that evolved  $W$  for  $t < 10M$  and  $\chi$  for  $t > 10M$  showed inaccuracies similar to the pure  $W$  system. At higher resolution  $W$  and  $\chi$  agreed with good accuracy. In Ref. [64] it was shown that this choice of gauge leads to a strongly hyperbolic evolution system provided that the shift does not become too large.

We use AHFINDERDIRECT [65] to locate apparent horizons. We measure the magnitude of the horizon spin using the Isolated Horizon algorithm detailed in [66]. This algorithm is based on finding an approximate rotational Killing vector (i.e. an approximate rotational symmetry) on the horizon, and given this approximate Killing vector  $\varphi^a$ , the spin magnitude is

$$S_{[\varphi]} = \frac{1}{8\pi} \oint_{AH} (\varphi^a R^b K_{ab}) d^2V \quad (4)$$

where  $K_{ab}$  is the extrinsic curvature of the 3D-slice,  $d^2V$  is the natural volume element intrinsic to the horizon, and  $R^a$  is the outward pointing unit vector normal to the horizon on the 3D-slice. We measure the direction of the spin by finding the coordinate line joining the poles of this Killing vector field using the technique introduced in [11]. Our algorithm for finding the poles of the Killing vector field has an accuracy of  $\sim 2^\circ$  (see [11] for details).

We also use an alternative quasi-local measurement of the spin and linear momentum of the individual black holes in the binary that is based on the coordinate rotation and translation vectors [40]. In this approach the spin components of the horizon are given by

$$S_{[i]} = \frac{1}{8\pi} \oint_{AH} \phi_{[i]}^\alpha R^b K_{ab} d^2V, \quad (5)$$

where  $\phi_{[\ell]}^i = \delta_{\ell j} \delta_{mk} r^m \epsilon^{ijk}$ , and  $r^m = x^m - x_0^m$  is the coordinate displacement from the centroid of the hole, while the linear momentum is given by

$$P_{[i]} = \frac{1}{8\pi} \oint_{AH} \xi_{[i]}^a R^b (K_{ab} - K \gamma_{ab}) d^2V, \quad (6)$$

where  $\xi_{[\ell]}^i = \delta_{\ell}^i$ .

We measure radiated energy, linear momentum, and angular momentum, in terms of  $\psi_4$ , using the formulae provided in Refs. [67, 68]. However, rather than using the full  $\psi_4$  we decompose it into  $\ell$  and  $m$  modes and solve for the radiated linear momentum, dropping terms with  $\ell \geq 5$ . The formulae in Refs. [67, 68] are valid at  $r = \infty$ . We obtain highly accurate values for these quantities by solving for them on spheres of finite radius (typically  $r/M = 50, 60, \dots, 100$ ), fitting the results to a polynomial dependence in  $l = 1/r$ , and extrapolating to  $l = 0$ . We perform fits based on a linear and quadratic dependence on  $l$ , and take the final values to be the quadratic extrapolation with the differences being the extrapolation error.

### A. Initial Data

We evolve quasi-circular configurations with a more massive spinning black hole, with specific spin  $a/m^H = 0.8$  pointing in the initial orbital plane, and a non-

spinning smaller BH. The orbital parameters were chosen using 3PN parameters for quasi-circular orbits with orbital period  $M\omega = 0.05$ , which provides the puncture locations and momenta. We normalize the puncture mass parameters so that the total ADM mass is  $1M$  and the mass ratio is the specified one. We then modify the configurations by rotating the initial spin direction (which has a small effect on the total ADM mass). We denote these configurations by QXXXTHYYY, where XXX denotes the mass ratio (XXX=100 for  $q = 1$ , XXX=66 for  $q = 2/3$ , XXX=50 for  $q = 1/2$ , XXX=40 for  $q = 1/2.5$ , XXX=33 for  $q = 1/3$ , and XXX=25 for  $q = 1/4$ ) and YYY gives the angle (in degrees) between the initial spin direction and the  $y$ -axis. The initial data parameters are summarized in Table I. These configurations have several advantages when modeling the out-of-plane kick as a function of mass ratio. First, one need only fit to two parameters (one angle and one amplitude) to determine the maximum recoil for a given mass ratio; improving the statistical reliability of the estimated maximum recoil. Second, the recoil velocity is quite large, even for  $q = 1/4$ , ensuring that errors in measuring the recoil velocity are not a significant fraction of the recoil itself. In addition the functional form used in our non-linear fits,  $A \cos(\vartheta - B)$ , yields a more robust measurement of  $A$  when compared to fits of  $C(\cos(\vartheta_1 - D) + E \cos(\vartheta_2 - F))$  (as used in Baker et al.) for small sample sizes (i.e. the functional form used here is more amenable to an accurate fit when the sample size is small). (See Fig. 5)

### B. Determining the Orbital Plane

These configurations show significant orbital precession, as demonstrated in Fig. 1, that presents a significant challenge when modeling the recoil. Our empirical formula (1) decomposes the recoil in terms of velocities parallel and perpendicular to the angular momentum. Thus we need an accurate determination of the orbital plane near merger (where most of the recoil is generated [38, 50]). In practice, we find a rotation, such that the late-time orbital plane is rotated onto the  $xy$ -plane. In order to model the out-of-plane recoil, we need to measure it as a function of the orientation of the spin vector during merger. We do this by fixing the remaining freedom in the transformation such that the transformed trajectories (for a given sequence of configurations) coincide (approximately) near merger. We then measure the spin direction at some fixed fiducial point along the merger trajectory (in practice, at the point  $r_0$  discussed below) and fit the out-of-plane kick to the form  $V = A \cos(\vartheta - B)$ , where  $\vartheta$  is the angle between the in-plane component of the spin at this fiducial point for a given configuration with the in-plane spin for the corresponding QXXXTH000 configuration.

We determine the orbital plane during merger in the

following way. We plot  $r = |\vec{r}_1 - \vec{r}_2|$  as a function of time and determine the location of the maximum of  $|\dot{r}|$ . We then choose two points on either side of the maximum with similar values of  $|\dot{r}|$  and a third point close to the maximum. We denote these three points of the trajectory with  $\vec{r}_+$ ,  $\vec{r}_0$ , and  $\vec{r}_-$ . We then choose a rotation such that the vector  $\vec{r}_a = \vec{r}_+ - \vec{r}_0$  lies on the new  $y$ -axis and that the normal to the plane determined by  $\vec{r}_a$  and  $\vec{r}_b = \vec{r}_- - \vec{r}_0$  lies along the new  $z$ -axis. With these choices we uniquely determine a rotational transformation from the coordinates used by the code to coordinates where the plunging orbital plane coincides with the  $xy$  plane. This transformation also rotates the trajectories in the appropriate way such that trajectories with similar late-time dynamics will overlap during merger (this is a generalization of the procedure given in Ref. [43, 50]).

In Fig. 1 we show the orbital trajectory difference  $\vec{r}_1 - \vec{r}_2$  for the Q25TH000 and Q25TH210 configurations. Note the significant precession and that the orbital planes near merger do not coincide. Fig. 2 shows that, after rotating the plane, as described above, the merger trajectories coincide.

In Figs. 3 and 4 we show the  $xy$  projections of the trajectories for the Q25THYYY configurations before and after rotating the merger orbital plane. Note that prior to

TABLE I: Initial data parameters for the quasi-circular configurations with a non-spinning smaller mass black hole (labeled 1), and a larger spinning black hole (labeled 2). The punctures are located at  $\vec{r}_1 = (x_1, 0, 0)$  and  $\vec{r}_2 = (x_2, 0, 0)$ , with momenta  $P = \pm(0, P, 0)$ , spins  $\vec{S}_2 = (S_x, S_y, 0)$ , mass parameters  $m^p$ , horizon (Christodoulou) masses  $m^H$ , and total ADM mass  $M_{\text{ADM}}$ . The configuration are denoted by QXXXTHYYY where XXX gives the mass ratio (0.25, 0.40, 0.33, 0.50, 0.66, 1.00) and YYY gives the angle in degrees between the initial spin direction and the  $y$ -axis. In all cases the initial orbital period is  $M\omega = 0.05$ .

Config	$x_1/M$	$x_2/M$	$P/M$	$m_1^p$	$m_2^p$	$S_x/M^2$	$S_y/M^2$	$m_1^H$	$m_2^H$	$M_{\text{ADM}}/M$	$a/m^H$
Q25TH000	5.18788	-1.27783	0.086696	0.18588	0.49511	0.00000	0.52144	0.20081	0.80326	1.00000	0.8082
Q25TH090	5.18788	-1.27783	0.086696	0.18588	0.49511	-0.52144	0.00000	0.20094	0.80324	1.00000	0.8082
Q25TH130	5.18788	-1.27783	0.086696	0.18588	0.49511	-0.39945	-0.33518	0.20080	0.80325	1.00000	0.8082
Q25TH210	5.18788	-1.27783	0.086696	0.18588	0.49511	0.26072	-0.45158	0.20081	0.80325	1.00000	0.8082
Q25TH315	5.18788	-1.27783	0.086696	0.18588	0.49511	0.36871	0.36871	0.20081	0.80325	1.00000	0.8032
Q33TH000	4.88556	-1.60904	0.101152	0.23415	0.46316	0.00000	0.45982	0.25147	0.75443	1.00000	0.8079
Q33TH090	4.88556	-1.60904	0.101152	0.23415	0.46316	-0.45982	0.00000	0.25144	0.75437	0.99994	0.8080
Q33TH130	4.88556	-1.60904	0.101152	0.23415	0.46316	-0.35224	-0.29557	0.25145	0.75440	0.99996	0.8080
Q33TH210	4.88556	-1.60904	0.101152	0.23415	0.46316	0.22991	-0.39822	0.25162	0.75443	0.99998	0.8079
Q33TH315	4.88556	-1.60904	0.101152	0.23415	0.46316	0.32514	0.32514	0.25145	0.75441	0.99997	0.8080
Q40TH000	4.66490	-1.84716	0.109810	0.26900	0.44033	0.00000	0.41792	0.28772	0.71930	1.00000	0.8077
Q40TH090	4.66490	-1.84716	0.109810	0.26900	0.44033	-0.41792	0.00000	0.28771	0.71927	0.99990	0.8079
Q40TH130	4.66490	-1.84716	0.109810	0.26900	0.44033	-0.32014	-0.26863	0.28771	0.71927	0.99994	0.8078
Q40TH210	4.66490	-1.84716	0.109810	0.26900	0.44033	0.20896	-0.36193	0.28771	0.71929	0.99997	0.8077
Q40TH315	4.66490	-1.84716	0.109810	0.26900	0.44033	0.29551	0.29551	0.28771	0.71929	0.99995	0.8078
Q50TH000	4.36532	-2.16588	0.119233	0.31591	0.40994	0.00000	0.36487	0.33611	0.67223	1.00001	0.8074
Q50TH090	4.36532	-2.16588	0.119233	0.31591	0.40994	-0.36487	0.00000	0.33609	0.67217	0.99984	0.8076
Q50TH130	4.36532	-2.16588	0.119233	0.31591	0.40994	-0.27950	-0.23453	0.33611	0.67220	0.99991	0.8076
Q50TH210	4.36532	-2.16588	0.119233	0.31591	0.40994	0.18243	-0.31598	0.33611	0.67222	0.99997	0.8074
Q50TH315	4.36532	-2.16588	0.119233	0.31591	0.40994	0.25800	0.25800	0.33613	0.67221	0.99993	0.8075
Q66TH000	3.93712	-2.61286	0.128421	0.38234	0.36743	0.00000	0.29620	0.40390	0.60587	1.00000	0.8069
Q66TH090	3.93712	-2.61286	0.128421	0.38234	0.36743	-0.29620	0.00000	0.40389	0.60579	0.99975	0.8072
Q66TH130	3.93712	-2.61286	0.128421	0.38234	0.36743	-0.22690	-0.19039	0.40388	0.60582	0.99985	0.8071
Q66TH210	3.93712	-2.61286	0.128421	0.38234	0.36743	0.14810	-0.25651	0.40389	0.60585	0.99994	0.8070
Q66TH315	3.93712	-2.61286	0.128421	0.38234	0.36743	0.20944	0.20944	0.40389	0.60583	0.99988	0.8071
Q100TH000	3.28027	-3.28027	0.133568	0.48338	0.30398	0.00000	0.20595	0.50543	0.50547	1.00001	0.8061
Q100TH090	3.28027	-3.28027	0.133568	0.48338	0.30398	-0.20595	0.00000	0.50541	0.50537	0.99965	0.8065
Q100TH130	3.28027	-3.28027	0.133568	0.48338	0.30398	-0.15777	-0.13238	0.50542	0.50541	0.99980	0.8063
Q100TH210	3.28027	-3.28027	0.133568	0.48338	0.30398	0.10297	-0.17836	0.50543	0.50544	0.99992	0.8062
Q100TH315	3.28027	-3.28027	0.133568	0.48338	0.30398	0.14563	0.14563	0.50542	0.50542	0.99983	0.8063

this transformation, there is no rotation in the  $xy$  plane that will make the late-time trajectories overlap and the reasonable overlap of the late-time trajectories for the transformed case.

### III. RESULTS

We used the following grid configurations for the runs. For the  $q = 1/2$ ,  $q = 1/2.5$ , and  $q = 1/3$  runs we placed the outer boundaries at  $1664M$  with a coarsest resolution of  $h = 25.6M$ , we used 12 levels of refinement around the smaller BH, with finest resolution of  $h = M/80$ , and 11 levels of refinement around the larger BH. For the  $q = 1/4$  runs we added an additional level of refinement

around the smaller BH and for the  $q = 2/3$  runs we added an additional level of refinement about the larger BH. For the  $q = 1$  runs we used 11 levels of refinement around the non-spinning hole and 12 levels of refinement around the spinning hole. In the  $q = 1/4$  case, we found that using eighth-order accuracy was critical, as incorrect dynamics (outspiral rather than inspiral when evolving with  $\chi$ , and plunges rather than inspirals when evolving with  $W$ ) resulted when using fourth order methods. The dynamics obtained from the  $W$  and  $\chi$  systems agreed when using eighth-order methods. In all cases we used  $\sigma = 3$  in the Gamma-driver shift condition.

In Table II we give the radiated energy and angular momenta for all configurations, as well as the untransformed recoil velocities.

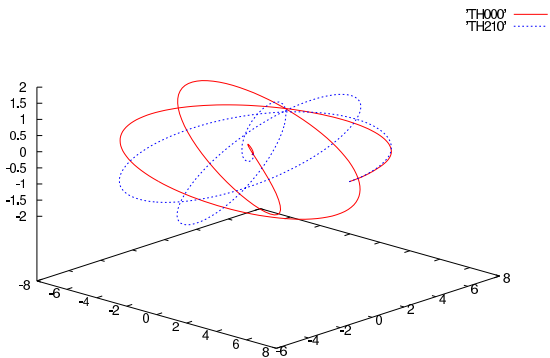


FIG. 1: The trajectory  $\vec{r}_1 - \vec{r}_2$  for the Q25TH000 and Q25TH210 configurations. Note the significant precession and the lack of alignment between the late-time orbital planes.

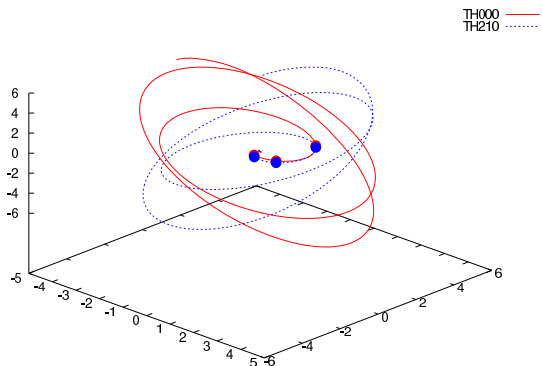


FIG. 2: The trajectory  $\vec{r}_1 - \vec{r}_2$  for the Q25TH000 and Q25TH210 configurations after rotating the system. Note the good agreement in the late time trajectories and that these trajectories now lie on the  $xy$  plane. The solid points are the locations of  $\vec{r}_+$ ,  $\vec{r}_0$ , and  $\vec{r}_-$ . Note that these points agree for both curves.

In order to measure the dependence of our recoil calculations on the choice of  $r_+$ ,  $r_0$ ,  $r_-$  (the three points in the trajectory that define the late-time orbital plane) we make two fiducial choices for these quantities  $(r_+, r_0, r_-)/M = (2.0, 1.0, 0.5)$  and  $(r_+, r_0, r_-)/M = (2.2, 1.2, 0.7)$ . In Table III we show how these two choices affect the calculation of  $v_{\parallel}$  and  $v_{\perp}$ , the spin component in and out of the plane, and the angle between the in-plane spins with the corresponding spin for the TH000 configurations ( $\vartheta$ ). Note that we report the magnitude of the in-plane (i.e.  $v_{\perp}$ ) recoil and spin  $a_{\perp}$ , because mod-

ifying  $(r_+, r_0, r_-)$  introduces additional rotations within the orbital plane; making a direct comparison of  $x$  and  $y$  components meaningless. Note that there is scatter in both the in-plane and out-of-plane components of the spin. The scatter in the out-of-plane component appears to be significant due to its small average value. The source of this scatter may simply be due to errors in estimated the true direction of the orbital plane (since the spin in the plane is large). We take the average value of the in-plane spin when fitting to Eq. (1) below.

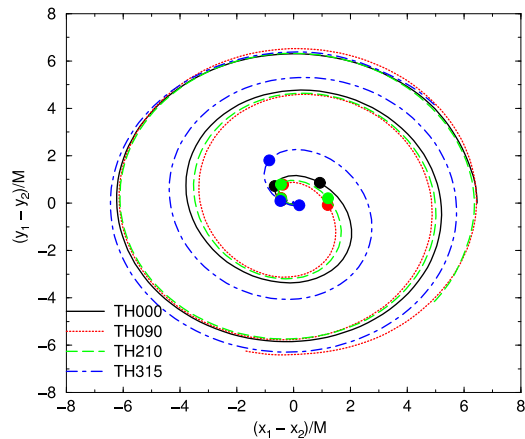


FIG. 3: The  $xy$  projection for the untransformed trajectory  $\vec{r}_1 - \vec{r}_2$  for the Q25THYYY configurations. The trajectories have been rotated (in the  $xy$  plane). Note that there are no rotations in the  $xy$  plane that will make the late-time trajectories overlap. The filled circles are the locations of  $\vec{r}_+$ ,  $\vec{r}_0$ , and  $\vec{r}_-$ .

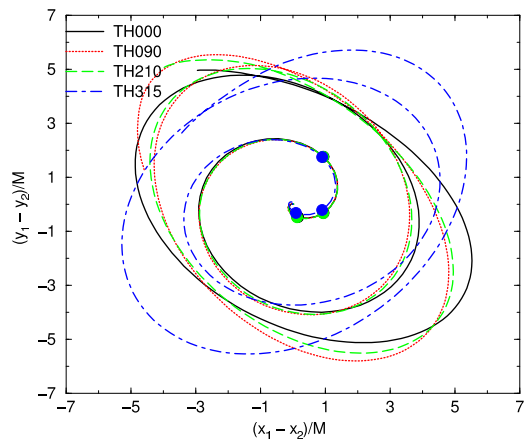


FIG. 4: The  $xy$  projection for the transformed trajectory  $\vec{r}_1 - \vec{r}_2$  for the Q25THYYY configurations. No additional rotations have been applied. Note the good agreement in the late time trajectories. The filled circles are the locations of  $\vec{r}_+$ ,  $\vec{r}_0$ , and  $\vec{r}_-$ .

Our empirical formula (1) predicts that  $v_{\parallel}$  will scale as  $\cos(\vartheta - \vartheta_0)$ . For each set of configurations with a given mass ratio, we perform a non-linear least squares fit of  $v_{\parallel}$  to the form  $v_{\parallel} = A \cos(\vartheta - B)$  and solve for  $A$  and  $B$ .

The results of these fits are summarized in Table IV. In Fig. 5 we plot the individual data points for each mass ratio and the best fit function.

With the above results we can now fit the maximum out-of-plane recoil ( $v_{\parallel}$ ) versus  $q$ . Our empirical for-

mula (1) predicts that this maximum will have the form  $v_{\parallel} = K\eta^2/(1+q)(\alpha_1 - q\alpha_2)$ , where  $\eta = q/(1+q)^2$ .

FIG. 5: A fit of  $v_{\parallel}$  for the  $q = 1, 2/3, 1/2, 1/2.5, 1/3, 1/4$  runs (from top to bottom) with the plane chosen by the points on the trajectory with  $(r_+, r_0, r_-) = (2, 1, 0.5)$  (left) and  $(r_+, r_0, r_-) = (2.2, 1.2, 0.7)$  (right).

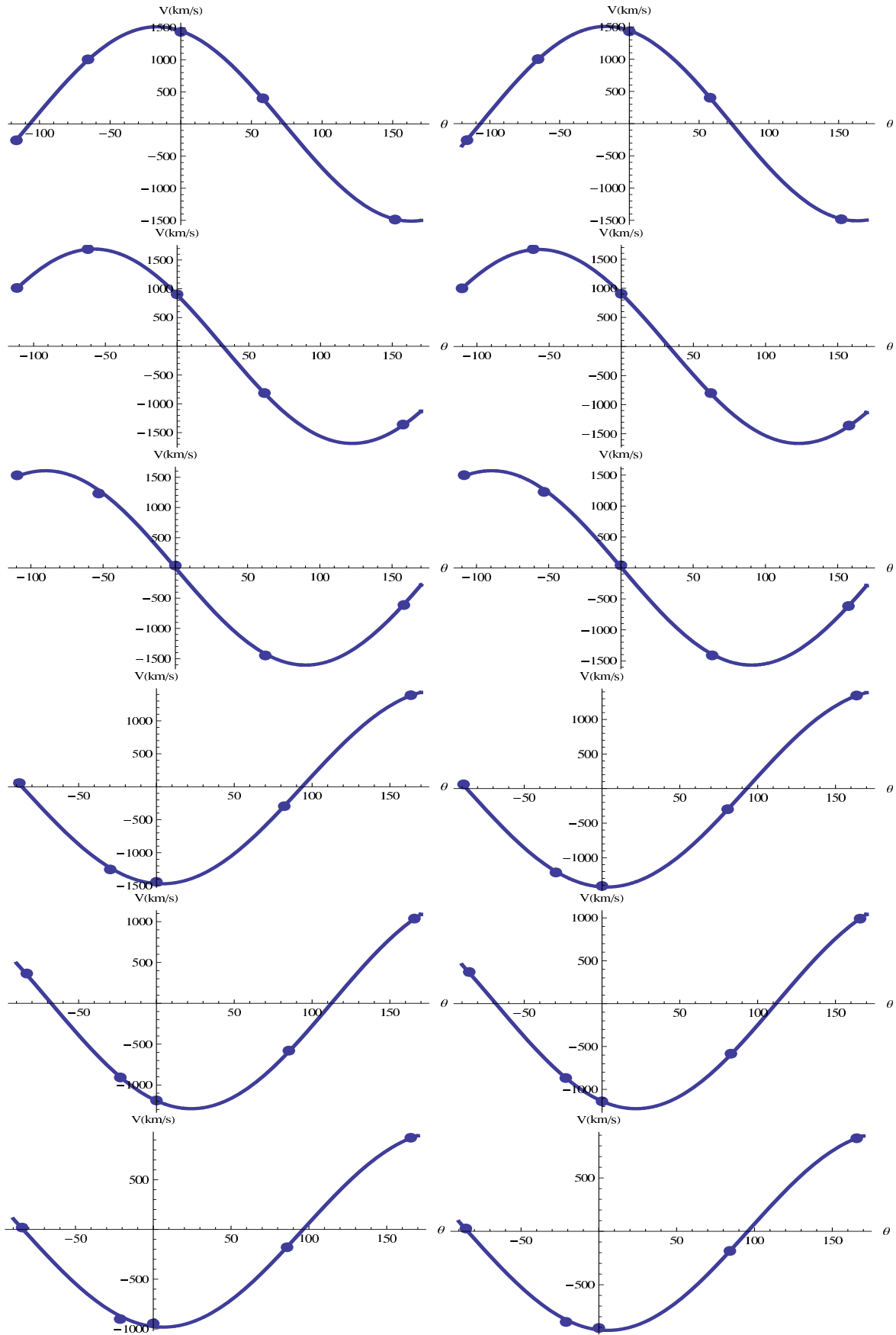


TABLE II: The radiated energy and angular momentum, as well as the recoil velocities for each configuration. Note that some of the error estimates, which are based on the differences between a linear and quadratic extrapolation in  $l = 1/r$ , are very small. This indicates that the error estimate is strongly underestimated the true error. All quantities are given in the coordinate system used by the code (i.e. the untransformed system).

Config	$100E/M$	$100J_x/M^2$	$100J_y/M^2$	$100J_z/M^2$	$V_x$	$V_y$	$V_z$
Q25TH000	$1.621 \pm 0.020$	$4.543 \pm 0.135$	$5.521 \pm 0.044$	$7.571 \pm 0.115$	$142 \pm 13$	$862 \pm 23$	$524 \pm 12$
Q25TH090	$1.642 \pm 0.016$	$-5.895 \pm 0.076$	$4.412 \pm 0.039$	$7.868 \pm 0.233$	$-877 \pm 21$	$98 \pm 15$	$477.8 \pm 7.0$
Q25TH130	$1.530 \pm 0.012$	$-6.879 \pm 0.040$	$-0.096 \pm 0.005$	$7.400 \pm 0.209$	$-77.7 \pm 8.2$	$-131.6 \pm 2.1$	$-102.5 \pm 3.9$
Q25TH210	$1.638 \pm 0.018$	$-1.045 \pm 0.106$	$-7.132 \pm 0.021$	$7.776 \pm 0.062$	$-340 \pm 23$	$818 \pm 19$	$-498.9 \pm 7.5$
Q25TH315	$1.512 \pm 0.014$	$6.774 \pm 0.063$	$0.583 \pm 0.030$	$7.375 \pm 0.188$	$63.7 \pm 8.5$	$-36.3 \pm 1.8$	$195.4 \pm 5.5$
Q33TH000	$2.216 \pm 0.023$	$4.731 \pm 0.073$	$7.171 \pm 0.087$	$11.516 \pm 0.098$	$47 \pm 19$	$989 \pm 21$	$814 \pm 11$
Q33TH090	$2.184 \pm 0.018$	$-7.569 \pm 0.026$	$4.653 \pm 0.040$	$11.548 \pm 0.082$	$-835 \pm 22$	$-25 \pm 15$	$611.9 \pm 7.7$
Q33TH130	$2.050 \pm 0.016$	$-8.485 \pm 0.017$	$-0.840 \pm 0.053$	$11.108 \pm 0.089$	$163.2 \pm 8.0$	$21.0 \pm 3.2$	$-342.7 \pm 1.4$
Q33TH210	$2.200 \pm 0.020$	$-0.433 \pm 0.081$	$-8.597 \pm 0.062$	$11.515 \pm 0.032$	$-449 \pm 27$	$798 \pm 13$	$-704.2 \pm 8.3$
Q33TH315	$2.054 \pm 0.017$	$8.335 \pm 0.022$	$1.495 \pm 0.010$	$11.072 \pm 0.002$	$297.8 \pm 6.9$	$167.2 \pm 8.5$	$489.38 \pm 0.71$
Q40TH000	$2.613 \pm 0.021$	$4.604 \pm 0.114$	$8.337 \pm 0.024$	$14.791 \pm 0.074$	$20 \pm 21$	$992 \pm 17$	$1119.8 \pm 5.0$
Q40TH090	$2.607 \pm 0.017$	$-8.761 \pm 0.001$	$4.729 \pm 0.133$	$14.790 \pm 0.147$	$-935 \pm 20$	$-73 \pm 12$	$975.1 \pm 6.8$
Q40TH130	$2.452 \pm 0.012$	$-9.332 \pm 0.033$	$-1.734 \pm 0.082$	$14.123 \pm 0.130$	$-21.3 \pm 4.7$	$-159.7 \pm 3.0$	$-104.6 \pm 4.7$
Q40TH210	$2.621 \pm 0.018$	$0.157 \pm 0.047$	$-9.604 \pm 0.013$	$14.815 \pm 0.072$	$-519 \pm 23$	$849.7 \pm 11.9$	$-1075.8 \pm 6.3$
Q40TH315	$2.441 \pm 0.014$	$9.165 \pm 0.068$	$2.464 \pm 0.083$	$13.933 \pm 0.039$	$109.5 \pm 2.2$	$-31.9 \pm 1.7$	$298.033 \pm 4.1$
Q50TH000	$2.814 \pm 0.013$	$4.089 \pm 0.0848$	$7.762 \pm 0.092$	$16.672 \pm 0.023$	$-113.0 \pm 3.4$	$163.6 \pm 9.9$	$-88.8 \pm 7.5$
Q50TH090	$2.865 \pm 0.018$	$-8.094 \pm 0.0421$	$4.566 \pm 0.198$	$17.499 \pm 0.336$	$619.51 \pm 0.37$	$-65 \pm 15$	$-1084.1 \pm 9.8$
Q50TH130	$2.991 \pm 0.017$	$-9.082 \pm 0.1534$	$-2.150 \pm 0.025$	$17.597 \pm 0.114$	$679.6 \pm 2.7$	$616 \pm 24$	$-1298.7 \pm 3.3$
Q50TH210	$2.805 \pm 0.014$	$0.087 \pm 0.0538$	$-8.922 \pm 0.098$	$16.83 \pm 0.089$	$9.5 \pm 6.8$	$-217.7 \pm 8.2$	$584.3 \pm 9.9$
Q50TH315	$2.985 \pm 0.018$	$8.788 \pm 0.1391$	$2.945 \pm 0.0222$	$17.43 \pm 0.0177$	$592.6 \pm 3.6$	$670 \pm 23$	$1224.39 \pm 0.79$
Q66TH000	$3.277 \pm 0.012$	$3.404 \pm 0.1164$	$7.633 \pm 0.0533$	$20.177 \pm 0.193$	$-69.0 \pm 4.7$	$-291.1 \pm 4.8$	$-861.6 \pm 8.3$
Q66TH090	$3.419 \pm 0.013$	$-8.028 \pm 0.0443$	$3.166 \pm 0.2086$	$21.293 \pm 0.133$	$743.8 \pm 5.3$	$17.67 \pm 15.06$	$-1539.46 \pm 15.31$
Q66TH130	$3.344 \pm 0.012$	$-7.896 \pm 0.1482$	$-2.756 \pm 0.2232$	$20.736 \pm 0.060$	$348.8 \pm 3.4$	$422.8 \pm 18.6$	$-916.1 \pm 8.7$
Q66TH210	$3.336 \pm 0.013$	$0.927 \pm 0.1165$	$-8.427 \pm 0.0148$	$20.701 \pm 0.048$	$226.0 \pm 2.9$	$-480.6 \pm 2.8$	$1263.6 \pm 12.3$
Q66TH315	$3.321 \pm 0.011$	$7.628 \pm 0.1358$	$3.368 \pm 0.1800$	$20.651 \pm 0.087$	$253.3 \pm 2.5$	$402.3 \pm 17.3$	$727.2 \pm 3.0$
Q100TH000	$3.580 \pm 0.006$	$2.036 \pm 0.1025$	$6.224 \pm 0.0869$	$23.232 \pm 0.038$	$-13.9 \pm 3.0$	$-445.1 \pm 3.2$	$-1366.1 \pm 2.8$
Q100TH090	$3.538 \pm 0.004$	$-6.452 \pm 0.2779$	$2.110 \pm 0.2082$	$23.541 \pm 0.332$	$347.3 \pm 0.9$	$24.3 \pm 3.1$	$-952.5 \pm 2.0$
Q100TH130	$3.461 \pm 0.001$	$-6.393 \pm 0.3509$	$-2.042 \pm 0.3155$	$22.749 \pm 0.003$	$-40.5 \pm 0.8$	$-2.4 \pm 6.2$	$256.9 \pm 3.5$
Q100TH210	$3.606 \pm 0.011$	$1.268 \pm 0.0057$	$-6.940 \pm 0.5645$	$23.382 \pm 0.072$	$232.4 \pm 5.9$	$-415.5 \pm 4.7$	$1412.8 \pm 1.0$
Q100TH315	$3.466 \pm 0.001$	$6.268 \pm 0.4289$	$2.608 \pm 0.2515$	$22.748 \pm 0.035$	$-72.6 \pm 0.7$	$-43.9 \pm 7.3$	$-395.6 \pm 4.2$



TABLE III: The transformed spin (at  $r = r_0$ ), recoil velocities in  $\text{km s}^{-1}$ , and angles between the in-plane QXXXTH000 spins and the other QXXXTHYYY configurations in degrees. A ‘1’ denotes a quantity measured using  $(r_+, r_0, r_-)/M = (2.0, 1.0, 0.5)$ , while a ‘2’ denotes a quantity measured using  $(r_+, r_0, r_-)/M = (2.2, 1.2, 0.7)$ . The differences between the values given for  $(2.0, 1.0, 0.5)$  and  $(2.2, 1.2, 0.7)$  are indicative of the errors. Note that in the transformed system  $L_z$  and  $S_z$  are both negative (i.e. there is some partial spin/orbit alignment). We denote quantities in the (transformed) orbital plane with an  $\perp$  subscript.

Config	$V_{\perp}(1)$	$V_{\parallel}(1)$	$a_{\perp}/m^H(1)$	$a_{\parallel}/m^H(1)$	$\vartheta(1)$	$V_{\perp}(2)$	$V_{\parallel}(2)$	$a_{\perp}/m^H(2)$	$a_{\parallel}/m^H(2)$	$\vartheta(2)$
Q25TH000	381.906	-944.218	0.765151	-0.220123	0	467.226	-905.041	0.777519	-0.171392	0
Q25TH090	442.087	-900.734	0.778871	-0.155682	-21.2857	535.91	-848.271	0.782551	-0.135979	-21.0555
Q25TH130	182.998	18.8238	0.770647	-0.202858	-84.2701	182.124	25.9541	0.759915	-0.247894	-85.4253
Q25TH210	428.772	921.968	0.773296	-0.18811	165.452	523.804	871.493	0.779785	-0.159086	165.72
Q25TH315	108.067	-178.557	0.763117	-0.233291	85.9471	99.6243	-183.401	0.743877	-0.288824	84.2327
Q33TH000	480.008	-1188.92	0.785384	-0.144133	0	588.18	-1139.3	0.787124	-0.134308	0
Q33TH090	499.061	-907.677	0.795365	-0.0836301	-23.2403	566.017	-867.504	0.792716	-0.105829	-23.2941
Q33TH130	107.877	364.575	0.754769	-0.264995	-83.3346	91.7575	368.962	0.753714	-0.275061	-85.3148
Q33TH210	507.918	1037.7	0.793736	-0.0993901	165.757	594.623	990.569	0.792668	-0.107581	165.86
Q33TH315	143.383	-579.277	0.747532	-0.285608	85.1084	126.005	-583.303	0.739378	-0.306098	82.8364
Q40TH000	394.333	-1442.99	0.782576	-0.177756	0	501.074	-1409.48	0.792558	-0.121423	0
Q40TH090	507.115	-1254.4	0.797605	-0.0811617	-29.708	599.055	-1213.19	0.798469	-0.074772	-29.6255
Q40TH130	183.684	56.2451	0.773172	-0.20708	-88.1121	182.148	61.0372	0.767006	-0.237119	-89.0041
Q40TH210	468.357	1388.93	0.794067	-0.117055	163.468	578.284	1346.88	0.797642	-0.0855529	163.572
Q40TH315	123.277	-294.347	0.762353	-0.243806	82.1551	112.97	-298.455	0.760328	-0.257681	80.7494
Q50TH000	214.284	38.4218	0.774399	-0.201633	0	213.369	43.2161	0.759323	-0.252543	0
Q50TH090	214.997	1231.73	0.770605	-0.229821	-53.0652	230.589	1228.91	0.774494	-0.21636	-53.2402
Q50TH130	428.04	1531.45	0.793283	-0.105245	-109.529	532.175	1498.45	0.800072	-0.06829	-108.518
Q50TH210	117.55	-612.411	0.752927	-0.272167	158.194	100.66	-615.412	0.743756	-0.296307	157.494
Q50TH315	456.63	-1446.08	0.799005	-0.0749945	62.2872	552.757	-1412.13	0.799513	-0.069376	63.1927
Q66TH000	124.717	903.442	0.763607	-0.251388	0	108.293	905.558	0.772394	-0.226846	0
Q66TH090	263.53	1689.39	0.7931	-0.116783	-62.1364	348.644	1673.9	0.802482	-0.066631	-60.9979
Q66TH130	334.035	1013.79	0.80055	-0.0605261	-111.577	374.13	999.887	0.797946	-0.0868091	-110.371
Q66TH210	170.848	-1360.02	0.770063	-0.232589	157.52	183.887	-1358.32	0.783732	-0.184392	157.808
Q66TH315	309.523	-811.859	0.798347	-0.0778683	60.8859	338.399	-800.253	0.795121	-0.109404	62.06
Q100TH000	85.6757	1434.26	0.79471	-0.158448	0	106.236	1432.88	0.800356	-0.116206	0
Q100TH090	124.676	1006.4	0.806191	-0.0286805	-65.6896	158.485	1001.63	0.803238	-0.0439484	-65.4866
Q100TH130	56.436	-253.872	0.785337	-0.163234	-116.365	45.8366	-255.999	0.785246	-0.170854	-116.398
Q100TH210	94.7375	-1487.81	0.805662	-0.0736974	151.702	148.253	-1483.43	0.804525	-0.0475139	151.917
Q100TH315	62.0569	399.755	0.78288	-0.178353	58.0786	47.7994	401.71	0.78611	-0.178897	57.8702

TABLE IV: Fit parameters for  $v_{\parallel} = A \cos((\vartheta - B)\pi/180)$  for each  $q$ .  $A$  is in units of  $\text{km s}^{-1}$  and  $B$  is in degrees. A (1) denotes values obtained from the  $(r_+, r_0, r_-) = (2, 1, 0.5)$  transformation, while a (2) denotes values obtained from the  $(r_+, r_0, r_-) = (2.2, 1.2, 0.7)$  transformation.

$q$	A(1)	B(1)	A(2)	B(2)
1/4	$982 \pm 17$	$186.3 \pm 1.0$	$927 \pm 10$	$185.69 \pm 0.68$
1/3	$1290.4 \pm 8.1$	$202.39 \pm 0.33$	$1224.9 \pm 5.2$	$201.75 \pm 0.23$
1/2.5	$1473 \pm 14$	$183.61 \pm 0.58$	$1424.9 \pm 8.2$	$183.00 \pm 0.35$
1/2	$1607 \pm 27$	$270.06 \pm 0.94$	$1570 \pm 19$	$270.45 \pm 0.70$
2/3	$1689.7 \pm 7.5$	$301.90 \pm 0.26$	$1666.8 \pm 6.7$	$302.934 \pm 0.24$
1	$1513.4 \pm 7.2$	$343.11 \pm 0.26$	$1507.9 \pm 5.3$	$343.18 \pm 0.19$

For all of our configurations  $\alpha_2 \approx 0$ , and hence  $v_{\parallel} = \alpha_1 K \eta^2 / (1 + q)$ . Interestingly, this form has a maximum

at  $q = 2/3$ . Baker et al. [53] propose that Eq. (1) should be modified to  $v_{\parallel} = 4K\eta^3 / (1 + q)(\alpha_1 - q\alpha_2)$  (which has a maximum at  $q = 3/4$  for fixed  $\alpha_1$  and  $\alpha_2 = 0$ ). In order to discriminate between these two possibilities we fit our data to the form

$$v_{\parallel}/\alpha = G\eta^H / (1 + q), \quad (7)$$

where we set  $G = K$  and  $4K$  and solve for  $H$ , as well as allowing both  $G$  and  $H$  to vary. Here  $\alpha = |\alpha_1^{\perp} - q\alpha_2^{\perp}|$ . It is important to note that our fits use six values of  $q$  to obtain one or two parameters. In Figs. 6, 7, and 8 we show results from these fits for the choices  $(r_+, r_0, r_-) = (2, 1, 0.5)$  and  $(r_+, r_0, r_-) = (2.2, 1.2, 0.7)$ . In the figures we plot the predicted recoil velocity using both our formula and the one proposed by Baker et al. assuming an uncertainty in  $K$  twice as large as that given in [3]. From the plots we can see that the

FIG. 6: Fit of out-of-plane recoil ( $V_{\parallel}/\alpha$ ) versus mass ratio  $q$  for the  $(r_+, r_0, r_-) = (2, 1, 0.5)$  choice of orbital plane. The top shaded region shows our predicted value for  $K = (6.0 \pm 0.2) \times 10^4$ , the lower region shows the prediction based on the modification proposed by Baker et al., the green curve shows a fit to  $\eta^n$ , while the blue curve has a simultaneous fit to  $\eta^n$  and  $K$ . Note that the measured values of  $V_{\parallel}/\alpha$ , while slightly overshooting the predictions, agree much better with our  $\mathcal{O}(\eta^2)$  form.

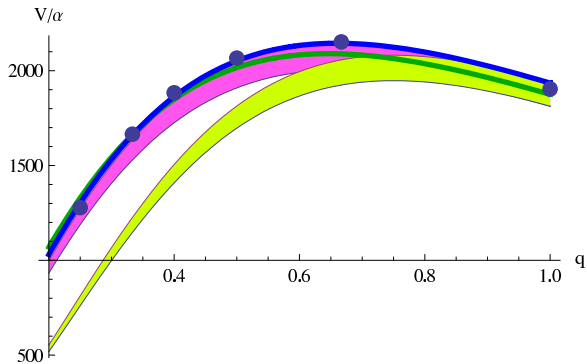
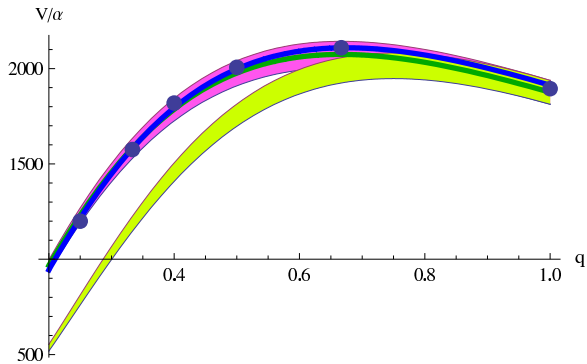
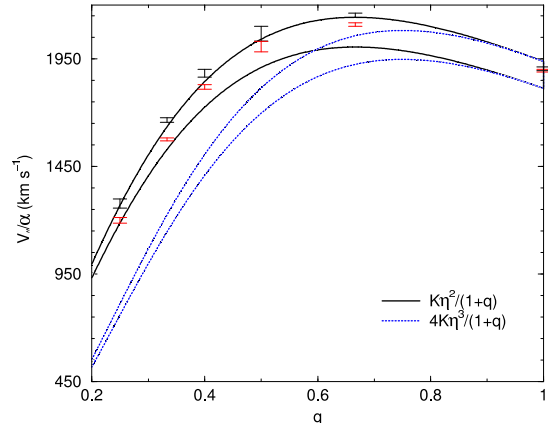


FIG. 7: Fit of out-of-plane recoil ( $V_{\parallel}/\alpha$ ) versus mass ratio  $q$  for the  $(r_+, r_0, r_-) = (2.2, 1.2, 0.7)$  choice of orbital plane. The top shaded region shows our predicted value for  $K = (6.0 \pm 0.2) \times 10^4$ , the lower region shows the prediction based on the modification proposed by Baker et al., the green curve shows a fit to  $\eta^n$ , while the blue curve has a simultaneous fit to  $\eta^n$  and  $K$ . Here we see very good agreement between the measured  $V_{\parallel}/\alpha$  and our prediction.



recoil velocities agree with our empirical formula much better than with the Baker et al. modification. The best fit functions have the form  $v_{\parallel}/\alpha = K\eta^{1.824 \pm 0.053}/(1+q)$  and  $v_{\parallel}/\alpha = K\eta^{1.994 \pm 0.036}/(1+q)$  for the choices  $(r_+, r_0, r_-) = (2, 1, 0.5)$  and  $(r_+, r_0, r_-) = (2.2, 1.2, 0.7)$  respectively, where  $K$  was set to  $K = 6.0 \times 10^4$ , and  $v_{\parallel}/\alpha = (61899 \pm 472)\eta^{1.941 \pm 0.039}/(1+q)$  and  $v_{\parallel}/\alpha = (61189 \pm 361)\eta^{2.070 \pm 0.031}/(1+q)$  respectively when both  $G$  and  $H$  are varied. The value of the constant  $K = G_{\text{fit}}$  determined in these latter two fits is in reasonable agreement with our previous measurement of  $K = (6.0 \pm 0.1) \times 10^4$ .

FIG. 8: The out-of-plane recoil ( $V_{\parallel}/\alpha$ ) versus mass ratio  $q$  for both choices of  $(r_+, r_0, r_-)$  as well as the predictions assuming a leading  $\eta^2$  and  $\eta^3$  dependence. The solid lines show the prediction assuming a leading  $\eta^2$  dependence and an error in  $K$  of  $0.2 \times 10^4 \text{ km s}^{-1}$ , while the dotted lines show the prediction assuming a leading  $\eta^3$  dependence and an error in  $K$  of  $0.2 \times 10^4 \text{ km s}^{-1}$ . The  $((r_+, r_0, r_-) = (2, 1, 0.5))$  data points lie above the  $((r_+, r_0, r_-) = (2.2, 1.2, 0.7))$  data points. The differences in these data points (for a given  $q$ ) is indicative of the true error in calculating the out-of-plane recoil.



### A. The In-Plane Kick

Examining Table III, we see that the magnitude of the in-plane recoil  $v_{\perp}$  is far larger than that predicted by Eq. (1) (the maximum predicted in-plane recoil velocity for the unequal mass cases is about 100 - 200  $\text{km s}^{-1}$  and is dominated by the unequal-mass, rather than spin, component of the recoil; while for the equal-mass case, the in-plane recoil is  $\sim 50 \text{ km s}^{-1}$ ), and that the difference in the magnitude for two choices of  $(r_+, r_0, r_-)$  are significant (around 25%). One possibility is simply that the direction of the orbital angular momentum was not measured with sufficient accuracy. If this is the case, then since the out-of-plane recoil is of order  $1000 \text{ km s}^{-1}$ , an error in the determination direction of the orbital angular momentum direction of  $20^\circ$ , would lead to an error in the in-plane recoil of  $350 \text{ km s}^{-1}$  (or 200%), but an error in the out-of-plane recoil of only  $60 \text{ km s}^{-1}$  (or 6%). Thus this seems to be a plausible explanation. However, as seen in Fig. 6 we appear to overestimate the out-of-plane recoil to a moderate degree. Another possible explanation is that the recoil due to unequal masses is a function of the acceleration of the masses, and is thus a function of the trajectories. Our trajectories differ significantly from the non-spinning, unequal mass trajectories. Thus Eq. (2a) may underestimate the unequal-mass component of the recoil in these cases. Finally we note that the unequal-mass component of the recoil is small due to cancellations in the radiated linear momentum between each half of the orbit. That is, the more symmetric the

orbit, the less net linear momentum radiated. Since our orbits precess, there is likely less cancellation.

#### IV. CONCLUSION

In this paper we explored the merger recoil from precessing black-hole binaries with a larger spinning black hole (with initial spin  $a/m = 0.8$ ) in quasi-circular orbit with a smaller non-spinning black hole. We introduced techniques to determine the normal to the orbital plane at merger and thus decompose the recoil into its in-plane and out-of plane components. However, there are important open questions about the accuracy of the determination of the orbital plane, the spin direction, and spin magnitude. All these quantities are measured in the highly dynamical region around the merger. In this work we have introduced techniques to begin studying this problem that will need to be refined. The issue of the in-plane recoil is particularly important, because large in-plane recoils imply that our heuristic formula needs to be

modified for strongly precessing binaries. Nevertheless, our results, as seen in Fig. 8, indicate that the out-of-plane recoil has an  $\mathcal{O}(\eta^2)$  rather than  $\mathcal{O}(\eta^3)$  leading-order dependence on the symmetric mass ration. This result, while agreeing with our prediction, appears to disagree with the recent work of Baker et al. [53]. Thus additional work with new configurations will be needed in order to determine leading-order dependence, or indeed, if this dependence is a function of the configuration.

#### Acknowledgments

We thank Manuela Campanelli for many valuable discussions. We gratefully acknowledge NSF for financial support from grant PHY-0722315, PHY-0701566, PHY 0714388, and PHY 0722703; and NASA for financial support from grant NASA 07-ATFP07-0158. Computational resources were provided by Lonestar cluster at TACC and by NewHorizons at RIT.

- 
- [1] S. Komossa, H. Zhou, and H. Lu, *Astrop. J. Letters* **678**, L81 (2008), 0804.4585.
  - [2] M. Campanelli, C. O. Lousto, Y. Zlochower, and D. Merritt, *Astrophys. J.* **659**, L5 (2007), gr-qc/0701164.
  - [3] M. Campanelli, C. O. Lousto, Y. Zlochower, and D. Merritt, *Phys. Rev. Lett.* **98**, 231102 (2007), gr-qc/0702133.
  - [4] F. Pretorius, *Phys. Rev. Lett.* **95**, 121101 (2005), gr-qc/0507014.
  - [5] M. Campanelli, C. O. Lousto, P. Marronetti, and Y. Zlochower, *Phys. Rev. Lett.* **96**, 111101 (2006), gr-qc/0511048.
  - [6] J. G. Baker, J. Centrella, D.-I. Choi, M. Koppitz, and J. van Meter, *Phys. Rev. Lett.* **96**, 111102 (2006), gr-qc/0511103.
  - [7] M. Campanelli, C. O. Lousto, and Y. Zlochower, *Phys. Rev. D* **73**, 061501(R) (2006).
  - [8] J. G. Baker, J. Centrella, D.-I. Choi, M. Koppitz, and J. van Meter, *Phys. Rev. D* **73**, 104002 (2006), gr-qc/0602026.
  - [9] M. Campanelli, C. O. Lousto, and Y. Zlochower, *Phys. Rev. D* **74**, 041501(R) (2006), gr-qc/0604012.
  - [10] M. Campanelli, C. O. Lousto, and Y. Zlochower, *Phys. Rev. D* **74**, 084023 (2006), astro-ph/0608275.
  - [11] M. Campanelli, C. O. Lousto, Y. Zlochower, B. Krishnan, and D. Merritt, *Phys. Rev.* **D75**, 064030 (2007), gr-qc/0612076.
  - [12] F. Pretorius, *Class. Quant. Grav.* **23**, S529 (2006), gr-qc/0602115.
  - [13] F. Pretorius and D. Khurana, *Class. Quant. Grav.* **24**, S83 (2007), gr-qc/0702084.
  - [14] J. G. Baker, J. R. van Meter, S. T. McWilliams, J. Centrella, and B. J. Kelly, *Phys. Rev. Lett.* **99**, 181101 (2007), gr-qc/0612024.
  - [15] B. Bruegmann et al. (2006), gr-qc/0610128.
  - [16] A. Buonanno, G. B. Cook, and F. Pretorius, *Phys. Rev.* **D75**, 124018 (2007), gr-qc/0610122.
  - [17] J. G. Baker et al., *Phys. Rev.* **D75**, 124024 (2007), gr-qc/0612117.
  - [18] M. A. Scheel et al., *Phys. Rev.* **D74**, 104006 (2006), gr-qc/0607056.
  - [19] J. G. Baker, M. Campanelli, F. Pretorius, and Y. Zlochower, *Class. Quant. Grav.* **24**, S25 (2007), gr-qc/0701016.
  - [20] P. Marronetti et al., *Class. Quant. Grav.* **24**, S43 (2007), gr-qc/0701123.
  - [21] H. P. Pfeiffer et al., *Class. Quant. Grav.* **24**, S59 (2007), gr-qc/0702106.
  - [22] J. A. González, M. D. Hannam, U. Sperhake, B. Bruggmann, and S. Husa, *Phys. Rev. Lett.* **98**, 231101 (2007), gr-qc/0702052.
  - [23] M. Campanelli, *Class. Quant. Grav.* **22**, S387 (2005), astro-ph/0411744.
  - [24] F. Herrmann, D. Shoemaker, and P. Laguna, *AIP Conf.* **873**, 89 (2006), gr-qc/0601026.
  - [25] J. G. Baker et al., *Astrophys. J.* **653**, L93 (2006), astro-ph/0603204.
  - [26] C. F. Sopuerta, N. Yunes, and P. Laguna, *Phys. Rev. D* **74**, 124010 (2006), astro-ph/0608600.
  - [27] J. A. González, U. Sperhake, B. Bruggmann, M. Hannam, and S. Husa, *Phys. Rev. Lett.* **98**, 091101 (2007), gr-qc/0610154.
  - [28] C. F. Sopuerta, N. Yunes, and P. Laguna, *Astrophys. J.* **656**, L9 (2007), astro-ph/0611110.
  - [29] F. Herrmann, I. Hinder, D. Shoemaker, and P. Laguna, *AIP Conf. Proc.* **873**, 89 (2006).
  - [30] F. Herrmann, I. Hinder, D. Shoemaker, and P. Laguna, *Class. Quant. Grav.* **24**, S33 (2007).
  - [31] F. Herrmann, I. Hinder, D. Shoemaker, P. Laguna, and R. A. Matzner, *Astrophys. J.* **661**, 430 (2007), gr-qc/0701143.
  - [32] M. Koppitz et al., *Phys. Rev. Lett.* **99**, 041102 (2007), gr-qc/0701163.

- [33] D.-I. Choi et al., Phys. Rev. **D76**, 104026 (2007), gr-qc/0702016.
- [34] J. G. Baker et al., Astrophys. J. **668**, 1140 (2007), astro-ph/0702390.
- [35] E. Berti et al., Phys. Rev. **D76**, 064034 (2007), gr-qc/0703053.
- [36] W. Tichy and P. Marronetti, Phys. Rev. **D76**, 061502 (2007), gr-qc/0703075.
- [37] F. Herrmann, I. Hinder, D. M. Shoemaker, P. Laguna, and R. A. Matzner, Phys. Rev. **D76**, 084032 (2007), arXiv:0706.2541 [gr-qc].
- [38] B. Brügmann, J. A. González, M. Hannam, S. Husa, and U. Sperhake (2007), arXiv:0707.0135 [gr-qc].
- [39] J. D. Schnittman et al. (2007), arXiv:0707.0301 [gr-qc].
- [40] B. Krishnan, C. O. Lousto, and Y. Zlochower, Phys. Rev. **D76**, 081501 (2007), arXiv:0707.0876 [gr-qc].
- [41] K. Holley-Bockelmann, K. Gultekin, D. Shoemaker, and N. Yunes (0700), arXiv:0707.1334 [astro-ph].
- [42] D. Pollney et al., Phys. Rev. D **76**, 124002 (2007), arXiv:0707.2559 [gr-qc].
- [43] S. Dain, C. O. Lousto, and Y. Zlochower (2008), 0803.0351.
- [44] I. H. Redmount and M. J. Rees, Comments on Astrophysics **14**, 165 (1989).
- [45] D. Merritt, M. Milosavljevic, M. Favata, S. A. Hughes, and D. E. Holz, Astrophys. J. **607**, L9 (2004), astro-ph/0402057.
- [46] A. Gualandris and D. Merritt (2007), arXiv:0708.0771 [astro-ph].
- [47] R. C. Kapoor, Pramana **7**, 334 (1976).
- [48] M. J. Fitchett, MNRAS **203**, 1049 (1983).
- [49] L. E. Kidder, Phys. Rev. D **52**, 821 (1995), gr-qc/9506022.
- [50] C. O. Lousto and Y. Zlochower, Phys. Rev. **D77**, 044028 (2008), arXiv:0708.4048 [gr-qc].
- [51] L. Boyle, M. Kesden, and S. Nissanke (2007), 0709.0299.
- [52] L. Boyle and M. Kesden (2007), 0712.2819.
- [53] J. G. Baker et al. (2008), arXiv:0802.0416 [astro-ph].
- [54] S. Brandt and B. Brügmann, Phys. Rev. Lett. **78**, 3606 (1997), gr-qc/9703066.
- [55] M. Ansorg, B. Brügmann, and W. Tichy, Phys. Rev. D **70**, 064011 (2004), gr-qc/0404056.
- [56] Y. Zlochower, J. G. Baker, M. Campanelli, and C. O. Lousto, Phys. Rev. D **72**, 024021 (2005), gr-qc/0505055.
- [57] T. Nakamura, K. Oohara, and Y. Kojima, Prog. Theor. Phys. Suppl. **90**, 1 (1987).
- [58] M. Shibata and T. Nakamura, Phys. Rev. D **52**, 5428 (1995).
- [59] T. W. Baumgarte and S. L. Shapiro, Phys. Rev. D **59**, 024007 (1999), gr-qc/9810065.
- [60] P. Marronetti, W. Tichy, B. Brügmann, J. González, and U. Sperhake (2007), arXiv:0709.2160 [gr-qc].
- [61] C. O. Lousto and Y. Zlochower, Phys. Rev. **D77**, 024034 (2008), arXiv:0711.1165 [gr-qc].
- [62] E. Schnetter, S. H. Hawley, and I. Hawke, Class. Quantum Grav. **21**, 1465 (2004), gr-qc/0310042.
- [63] M. Alcubierre, B. Brügmann, P. Diener, M. Koppitz, D. Pollney, E. Seidel, and R. Takahashi, Phys. Rev. D **67**, 084023 (2003), gr-qc/0206072.
- [64] C. Gundlach and J. M. Martin-Garcia, Phys. Rev. **D74**, 024016 (2006), gr-qc/0604035.
- [65] J. Thornburg, Class. Quantum Grav. **21**, 743 (2004), gr-qc/0306056.
- [66] O. Dreyer, B. Krishnan, D. Shoemaker, and E. Schnetter, Phys. Rev. D **67**, 024018 (2003), gr-qc/0206008.
- [67] M. Campanelli and C. O. Lousto, Phys. Rev. D **59**, 124022 (1999), gr-qc/9811019.
- [68] C. O. Lousto and Y. Zlochower, Phys. Rev. D **76**, 041502(R) (2007), gr-qc/0703061.